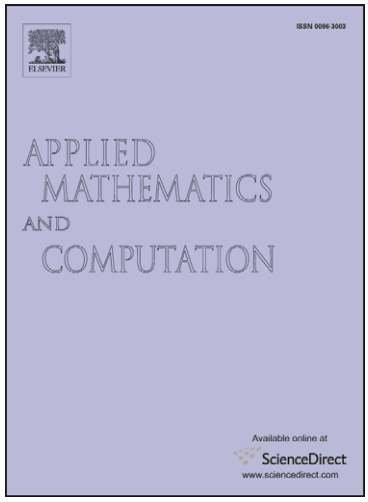

Nonlinear explicit analysis and study of the behaviour of a new ring-type brake energy dissipator by FEM and experimental comparison

J.J. del Coz Díaz, P.J. García Nieto, D. Castro-Fresno, J. Rodríguez-Hernández

PII: S0096-3003(10)00251-1
DOI: 10.1016/j.amc.2010.03.009
Reference: AMC 14801

To appear in: *Appl. Math. Comput.*

Please cite this article as: J.J. del Coz Díaz, P.J. García Nieto, D. Castro-Fresno, J. Rodríguez-Hernández, Nonlinear explicit analysis and study of the behaviour of a new ring-type brake energy dissipator by FEM and experimental comparison, *Appl. Math. Comput.* (2010), doi: 10.1016/j.amc.2010.03.009

Nonlinear explicit analysis and study of the behaviour of a new ring-type brake energy dissipator by FEM and experimental comparison

J. J. del Coz Díaz[a*], P. J. García Nieto[b], D. Castro-Fresno[c] and J. Rodríguez-Hernández[c]

[a]*Department of Construction, University of Oviedo, 33204 Gijón, Spain*
[b]*Department of Mathematics, University of Oviedo, 33007 Oviedo, Spain*
[c]*Department of Construction, University of Cantabria, 39005 Santander, Spain*

Abstract
The aim of this paper is to comprehensively analyse the performance of a new ring-type brake energy dissipator through the finite element method (FEM) (formulation and finite element approximation of contact in non-linear mechanics) and experimental comparison. This new structural device is used as a system component in rockfall barriers and fences and it is composed of steel bearing ropes, bent pipes and aluminium compression sleeves. The bearing ropes are guided through pipes bent into double-loops and held by compression sleeves. These elements work as brake rings. In important events the brake rings contract and so dissipate residual energy out of the ring net, without damaging the ropes. The rope's breaking load is not diminished by activation of the brake. The full understanding of this problem implies the simultaneous study of three non-linearities: material nonlinearity (plastic behaviour) and failure criteria, large displacements (geometric non-linearity) and friction-contact phenomena among brake ring components. The explicit dynamic analysis procedure is carried out by means of the implementation of an explicit integration rule together with the use of diagonal element mass matrices. The equations of motion for the brake ring are integrated using the explicit central difference integration rule. The presence of the contact phenomenon implies the existence of inequality constraints. The conditions for normal contact are $\lambda \geq 0$, $g \geq 0$ and $g\lambda = 0$, where λ is the normal traction component and g is the gap function for the contact surface pair. To include frictional conditions, let us assume that Coulomb's law of friction holds pointwise on the different contact surfaces, μ being the dynamic coefficient of friction. Next, we define the non-dimensional variable τ by means of the expression $\tau = t / \mu\lambda$, where $\mu\lambda$ is the frictional resistance and t is the tangential traction component. In order to find the best brake performance, different dynamic friction coefficients corresponding to the pressures of the compression sleeves have been adopted and simulated numerically by FEM and then we have compared them with the results from full-scale experimental tests. Finally, the most important conclusions of this study are given.

MSC2000 Codes: 74S05, 65L60, 65P99, 74M10, 49J40
Key words: Inequality constraints; Finite element analysis; Explicit integration; Elastoplastic material; Coulomb's law; Contact analysis; Weak solution

1. Introduction

The finite element method is a numerical procedure that can be used to obtain solutions to many engineering problems involving stress analysis, heat transfer, electromagnetism, and in our case, a new ring-type brake energy dissipator [1-6].

* Corresponding author. Tel.: +34-985-182042; fax: +34-985-182433.
E-mail address: juanjo@construi.uniovi.es (J. J. del Coz Díaz).

The main objective of this paper is to determine by FEM the absorbed energy and the failure modes in the different components of the brake. Then the FEM results are compared with experimental ones obtained by means of full-scale tests.

The bearing ropes are guided through pipes bent into double-loops and held by compression sleeves forming elements that work as brake rings. In large events the brake rings contract and so dissipate the residual energy out of the ring net, without damaging the ropes (see Fig. 1).

Fig. 1. Geometrical model of the new ring-type brake dissipator (left) and falling rock protection system (right).

The falling rock protection system consists of a product made of nets [4] (interception structure), posts (support structure), ropes (connection structure) and brakes (connection structure). The energy level of a falling rock protection kit is defined as the kinetic energy of a regular block impacting on the net fence. In this way, the energy dissipating device is the most important element in order to absorb energy and to avoid the rupture of the connection components, so that the complete separation occurs of the component itself into two distinct parts.

2. Strong form of the initial boundary value problem

An elastoplastic body occupies a bounded domain $\Omega \subset \Re^d \left(d = 2,3\right)$ with a Lipschitz boundary Γ, partitioned into three disjointed measurable parts Γ_u, Γ_σ and Γ_c so that $meas\left(\Gamma_u\right) > 0$ [7]. A volume force of density $\vec{f}^B$ acts in Ω and a surface traction of density $\vec{f}^S$ acts on Γ_σ. The body is clamped on Γ_u and thus the displacement and velocity fields vanish there. On Γ_c the body is in contact with other bodies, the so-called compression sleeves, bearing ropes and pipe bends. We model the contact with Coulomb's law of dry friction [5, 8-9]. Finally, M_d denotes the space of the second order symmetric tensors on $\Re^d$, or equivalently, the space of the symmetric matrices of order *d*.

The strong formulation of the contact problem is the following:

Problem 1. For all $t \in I\left[0,T\right]$ and all $\vec{x} \in \Omega$, find a displacement field $\vec{u}(\vec{x},t): \Omega \times \left[0,T\right] \to \Re^d$ and a stress field $\vec{\sigma}\left(\vec{x},t\right): \Omega \times \left[0,T\right] \to M_d$ so that they satisfy [10]:

1. Linear momentum balance:

$$\nabla \cdot \vec{\sigma} + \vec{f}^B = \rho \ddot{\vec{u}} \tag{1}$$

in direct notation and

$$\sigma_{ij,j} + f_i^B = \rho \ddot{u}_i \tag{2}$$

in indicial notation. In Eqs. (1) and (2), $\vec{\sigma}$ is the Cauchy stress tensor, σ_{ij}, f_i^B being the components of the applied body force per unit volume $\vec{f}^B$, and the scalar ρ denotes the mass density, which may in general depend on the coordinates $\vec{x} \in \Omega$. The two superposed dots on $\vec{u}$ denote partial differentiation with respect to time twice. The notation j in a subscript indicates partial differentiation of the quantity with respect to that coordinate direction.

2. Initial and boundary conditions:
In addition to the previous momentum balance, which must hold for any time $t \in I[0,T]$, the problem is in general subject to certain initial and boundary conditions as well. The boundary conditions are stated by introducing prescribed tractions $\bar{\vec{f}}^S : \Gamma_\sigma \times [0,T] \to \Re^d$ and prescribed displacements $\bar{\vec{u}} : \Gamma_u \times [0,T] \to \Re^d$ and requiring:

$$\sigma_{ij} n_j = \bar{f}_i^S \text{ for all } \vec{x} \in \Gamma_\sigma, t \in [0,T] \tag{3}$$

$$u_i = \bar{u}_i \text{ for all } \vec{x} \in \Gamma_u, t \in [0,T] \tag{4}$$

where n_j refers to the components of the outward normal $\vec{n}$ to Γ_σ. Initial conditions may be expressed by introducing an initial displacement field $\vec{u}_0 : \bar{\Omega} \to \Re^d$ and initial velocity field $\vec{v}_0 : \bar{\Omega} \to \Re^d$ where $\bar{\Omega}$ denotes the closure of the open set Ω; that is to say, including the boundary $\partial\Omega = \Gamma_u \cup \Gamma_\sigma \cup \Gamma_c$, and requiring:

$$u_i\big|_{t=0} = u_{0i} \text{ in } \bar{\Omega}, \tag{5}$$

$$\dot{u}_i\big|_{t=0} = v_{0i} \text{ in } \bar{\Omega} \tag{6}$$

3. Strain-displacement relationships:

$$\varepsilon_{ij} = \frac{1}{2}\left(u_{i,j} + u_{j,i}\right) \tag{7}$$

where ε_{ij} are the components of the strain tensor.

4. Constitutive relationships:
   - For linear elasticity:

$$\sigma_{ij} = c_{ijkl}\varepsilon_{kl} \tag{8}$$

   where c_{ijkl} is the fourth order elasticity tensor
   - For plasticity with kinematic/isotropic hardening:

$$\sigma_{ij} = c_{ijkl}\left(\varepsilon_{kl} - \varepsilon_{kl}^p\right) \tag{9}$$

   where ε_{kl}^p is the inelastic portion of strain. Then, we define the intermediate variable $\vec{\xi}$ as:

$$\xi_{ij} = \sigma'_{ij} - q_{ij} \tag{10}$$

where $\vec{\sigma}'$ is the deviatoric stress tensor and $\vec{q}$ is the deviatoric back stress tensor. Classically, if one selects an associative flow rule, this may be done in terms of a *consistency parameter* $\dot{\gamma}$ using:

$$\dot{\vec{\varepsilon}}^p = \dot{\gamma}\frac{\partial F}{\partial \vec{\sigma}} \tag{11}$$

where $\dot{\gamma}$ defines the magnitude of the rate of plastic flow and *F* denotes the yield function under consideration. For the von Mises description of plasticity, we have:

$$\dot{\vec{\varepsilon}}^p = \dot{\gamma}\frac{\vec{\sigma}'}{\left\|\vec{\sigma}'\right\|} \tag{12}$$

where $\left\|\vec{\sigma}'\right\| = \sqrt{\sigma'_{ij}\sigma'_{ij}}$. To enable greater generality, we may introduce a combination of kinematic and isotropic hardening through use of the parameter $\beta \in [0,1]$, a hardening modulus *H* and a hardening variable e^p. The evolution of e^p is defined in terms of the consistency parameter $\dot{\gamma}$ as:

$$\dot{e}^p = \left|\dot{\gamma}\right| \tag{13}$$

and the back stress $\vec{q}$ evolves according to:

$$\dot{\vec{q}} = \dot{\gamma}\frac{2}{3}(1-\beta)H\frac{\vec{\xi}}{\left\|\vec{\xi}\right\|} \tag{14}$$

The model is constructed so that pure isotropic hardening is produced when $\beta = 1$; pure kinematic hardening is produced when $\beta = 0$ and some combination occurs for intermediate values of β. This may be accomplished mathematically by replacing the yield function for perfect plasticity as follows:

$$\Phi(\vec{\sigma},\vec{q},e^p) = \left\|\vec{\xi}\right\| - \sqrt{\frac{2}{3}}\left[\sigma_Y + \beta\sqrt{\frac{2}{3}}He^p\right] \le 0 \tag{15}$$

when σ_Y is the uniaxial yield stress. With this choice of yield function, the flow rule in (12) must be altered slightly to read:

$$\dot{\vec{\varepsilon}}^p = \dot{\gamma}\frac{\vec{\xi}}{\left\|\vec{\xi}\right\|} \tag{16}$$

Finally, the model may be completed by specification of the so-called loading/unloading conditions for elastoplasticity. These may be given in terms of the classical Kuhn-Tucker conditions for inequality constraints in optimization:

$$\begin{cases} \Phi \le 0 \\ \dot{\gamma} \ge 0 \\ \dot{\gamma}\Phi = 0 \end{cases} \tag{17}$$

which ensure that; stresses and historic variables are not allowed to evolve to the extent that the stress point is outside the yield surface, the

magnitude of the plastic strain rate is always positive and plasticity only occurs when the stress point is on the yield surface. These are usually augmented with a persistency condition:

$$\dot{\Phi}\dot{\gamma} = 0 \tag{18}$$

which ensures that if elastic unloading begins to occur while a point is still on the yield surface, the plastic strain rate will be zero.

5. Contact conditions

The contact conditions interrelating the contact pressure, λ, and the gap function, g, on the contact surface Γ_c may now be stated in terms of Kuhn-Tucker optimality conditions, characteristic of problems involving inequality constraints [8, 11]:

$$\begin{cases} \lambda \geq 0 \\ g \leq 0 \\ \lambda g = 0 \end{cases} \tag{17}$$

which must hold for all $\vec{x} \in \Gamma_c$. The first equation (17) refers to the fact that all contact interaction must be compressive, while the second states the impenetrability condition. The final condition given in (17), the *complementarity condition*, requires that compressive stress only be generated in the instance where contact is occurring, i.e., when $g = 0$. When $g < 0$, this condition requires that λ be zero, consistent with an out-of-contact condition.

3. Variational formulation of the problem

One of the major areas of nonlinear analysis is the solution of problems in which separate bodies or structures may come in contact with each other. Several methods have been developed to handle such problems. A particularly difficult nonlinear behaviour to analyze is the contact between two or more bodies [1, 10]. Contact problems range from frictionless contact in small displacements to contact with friction in general large strain inelastic conditions, such as our case.

3.1. Contact conditions: continuum mechanics equations

Let us consider *N* bodies that are in contact at time *t*. Let Γ_c^t be the complete area of contact for each body L, $L = 1...N$; then the principle of virtual work for the *N* bodies at time *t* gives [1, 10, 12]:

$$\sum_{L=1}^{N}\left\{\int_{\Omega^t} \tau_{ij}^t \delta_t e_{ij} d\Omega^t\right\} = \sum_{L=1}^{N}\left\{\int_{\Omega^t} \delta u_i \left(f_i^B\right)^t d\Omega^t + \int_{\Gamma_\sigma^t} \delta u_i \left(f_i^S\right)^t d\Gamma^t\right\} + \sum_{L=1}^{N}\int_{\Gamma_c^t} \delta u_i^c \left(f_i^c\right)^t d\Gamma^t \tag{18}$$

where the part in brackets corresponds to the usual terms:

τ_{ij}^t = Cartesian components of the Cauchy stress tensor (force per unit area in the deformed geometry).

$\delta_t e_{ij}$ = strain tensor corresponding to virtual displacements.

δu_i = components of the virtual displacement vector imposed on configuration at time *t*, of a function of x_j^t, $j = 1,2,3...$

x_i^t = Cartesian coordinates of material point at time *t*.

Ω^t = volume at time *t*.

$\left(f_i^B\right)^t$ = components of externally applied forces per unit volume at time *t*.

$\left(f_i^S\right)^t$ = components of externally applied surface tractions per unit surface area at time *t*.

Γ_σ^t = surface at time *t* on which external tractions are applied.

$\delta u_i^S = \delta u_i$ evaluated on the surface Γ_σ^t (the δu_i components are zero and correspond to the prescribed displacements on the surface Γ_u^t).

and the last summation sign in Eq. (18) gives the contribution of the contact forces. The contact force effect is included as a contribution in the externally applied tractions. The components of the contact tractions are denoted as $\left(f_i^c\right)^t$ and act over the areas Γ_c^t (the actual area of contact for body at time *t*), and the components of the known externally applied tractions are denoted as $\left(f_i^S\right)^t$ and act over the areas Γ_σ^t. It can be assumed that the areas Γ_σ^t are not part of the areas Γ_c^t, although such an assumption is unnecessary.

Fig. 2. Bodies in contact at time *t*.

Fig. 2 illustrates schematically the case of two bodies, which are now considered in greater detail. In this paper, the two bodies in contact are denoted as body *I* and body *J*. Note that each body is supported so that without contact no rigid body motion is possible. Let $\left(\vec{f}^{IJ}\right)^t$ be the vector of contact surface tractions on body *I* due to contact with body *J*, then $\left(\vec{f}^{IJ}\right)^t = -\left(\vec{f}^{JI}\right)^t$. Hence, the virtual work due to the contact tractions in (18) can be written as [1, 10, 13]:

$$\int_{S^{IJ}} \delta u_i^I \left(f_i^{IJ}\right)^t dS^{IJ} + \int_{S^{JI}} \delta u_i^J \left(f_i^{JI}\right)^t dS^{JI} = \int_{S^{IJ}} \delta u_i^{IJ} \left(f_i^{IJ}\right)^t dS^{IJ} \qquad (19)$$

where δu_i^I and δu_i^J are the components of the virtual displacements on the contact surfaces of bodies *I* and *J*, respectively, and :

$$\delta u_i^{JI} = \delta u_i^I - \delta u_i^J \qquad (20)$$

The pair of surfaces S^{IJ} and S^{JI} are termed a 'contact surface pair'. Note that these surfaces are not necessarily of equal size. However, the actual area of contact at time *t* for body *I* is S_c^t of body *I*, and for body *J* it is S_c^t of body *J*, and in each case this area is part of S^{IJ} and S^{JI}. It is convenient to call S^{IJ} the 'contactor surface' and S^{JI} the 'target surface'. Therefore, the right-hand side of (18) can be interpreted as the virtual work that the contact tractions produce over the virtual relative displacements on the contact surface pair.

Let $\vec{n}$ be the unit outward normal to S^{JI} and let $\vec{s}$ be a vector so that $\vec{n}$ and $\vec{s}$ form a

right-hand basis (see Fig. 3 below). It is possible to decompose the contact tractions $\left(f^{IJ}\right)^t$ acting on S^{IJ} into normal and tangential components corresponding to $\vec{n}$ and $\vec{s}$ on S^{JI}:

$$\left(f^{IJ}\right)^t = \lambda\vec{n} + t\vec{s} \tag{21}$$

where λ and t are the normal and tangential traction components. Thus,

$$\lambda = \left[\left(\vec{f}^{IJ}\right)^t\right]^T \vec{n}\,;\; t = \left[\left(\vec{f}^{IJ}\right)^t\right]^T \vec{s} \tag{22}$$

In order to define the actual values of $\vec{n}$ and $\vec{s}$ that are used in the contact calculations, consider a generic point $\vec{x}$ on S^{IJ} and let $\vec{y}^*(\vec{x},t)$ be the point on S^{JI} satisfying:

$$\left\|\vec{x} - \vec{y}^*(\vec{x},t)\right\|_2 = \min_{\vec{y}\in S^{JI}} \left\{\left\|\vec{x} - \vec{y}\right\|_2\right\} \tag{23}$$

The distance from $\vec{x}$ to S^{JI} is then given by:

$$g(\vec{x},t) = \left(\vec{x} - \vec{y}^*\right)^T \vec{n}^* \tag{24}$$

where $\vec{n}^*$ is the unit *normal vector* that is used at $\vec{y}^*(\vec{x},t)$ (see Fig. 3 below) and $\vec{n}^*$, $\vec{s}^*$ are used in equation (21) corresponding to the point $\vec{x}$. The function g is the gap function for the contact surface pair.

Fig. 3. Definitions used in contact analysis.

With the above definitions, the conditions for normal contact are given by Eq. (17).
In order to include frictional conditions, let us assume that Coulomb's law of friction holds pointwise on the contact surface and μ is the coefficient of friction [10].

Let us define the non-dimensional variable τ given by:

$$\tau = \frac{t}{\mu\lambda} \tag{25}$$

where $\mu\lambda$ is the "frictional resistance", and the magnitude of the relative tangential velocity:

$$\dot{u}(\vec{x},t) = \left(\dot{\vec{u}}^J\Big|_{\vec{y}^*(\vec{x},t)} - \dot{\vec{u}}^I\Big|_{(\vec{x},t)}\right)\cdot\vec{s}^* \tag{26}$$

corresponding to the unit tangential vector $\vec{s}$ at $\vec{y}^*(\vec{x},t)$. Hence, $\dot{u}(\vec{x},t)\vec{s}^*$ is the tangential velocity at time t of the material point at $\vec{y}^*$ relative to the material point at $\vec{x}$. With these definitions Coulomb's law of friction states [1, 10]:

$$\begin{cases} |\tau| < 1 \\ |\tau| < 1 \Rightarrow \dot{u} = 0 \\ |\tau| = 1 \Rightarrow sign(\dot{u}) = sign(\tau) \end{cases} \tag{27}$$

Fig. 4. Interface conditions in contact analysis.

Fig. 4 illustrates these interface conditions. The solution of the contact problem in Fig. 4 therefore entails the solution of the virtual work equation (18) (specialized for bodies *I*

and *J*) subject to conditions (17) and (27).

3.2. Solution approach for contact problems

Let w be a function of g and λ such that the solutions of $w(g,\lambda)=0$ satisfy the conditions for normal contact (17), and similarly, let v be a function of τ and $\dot{u}$ such that the solutions of $v(\dot{u},\tau)=0$ satisfy the frictional conditions (27). Then, the contact conditions are given by:

$$w(g,\lambda)=0 \tag{28}$$

$$v(\dot{u},\tau)=0 \tag{29}$$

These conditions can now be imposed on the principle of the virtual work equation using a Penalty Approach (PA), Lagrange Multiplier Method (LMM) or Augmented Lagrangian Method (ALM) [14-17]. The variables λ and τ can be considered Lagrange multipliers, so let $\delta\lambda$ and $\delta\tau$ be variations in these quantities. Multiplying (28) by $\delta\lambda$ and (29) by $\delta\tau$ and integrating over S^{IJ} (the contactor surface), we obtain the constraint equation:

$$\int_{S^{IJ}} \left[\delta\lambda\, w(g,\lambda)+\delta\tau\, v(\dot{u},\tau)\right] dS^{IJ}=0 \tag{30}$$

In this work, we have used the ALM approach. In order to discretize the contact conditions, we have used the surface-to-surface contact elements. In summary, the governing equations to be solved for the two-body contact problem are the usual principle of virtual work (Eq. (18)), with the effect of the contact tractions included through externally applied (but unknown) forces, plus the constraint Eq. (30). The finite element solution of the governing continuum mechanics equations can be obtained by using the discretization procedures for the principle of virtual work, and also by discretizing the contact conditions.

4. Finite element model

Based on the geometric model previously described, the finite element model was built, following a four-step process [2, 18]:

- Definition of material properties and failure criteria.
- Selecting the element types, formulations and real constants.
- Meshing of the geometrical model.
- Applying loads and boundary conditions and obtaining the solution

The material properties adopted in our model are the following [19-20]:

- Steel (Johnson-Cook model): A bilinear kinematic hardening option was selected to describe the material behaviour and the data provided by the experimental tests (in the form of stress-strain curves) was curve-fitted to a multi-linear representation for the thin steel plate.

$$\sigma_y=\left[A+B\cdot\varepsilon_p^{n}\right]\cdot\left[1+C\ln\left|\dot{\varepsilon}_p^{*}\right|\right] \tag{31}$$

  The expression in the first set of brackets gives the stress as a function of strain when $\dot{\varepsilon}_p^{*}=1.0\,\mathrm{s}^{-1}$, where ε_p is the effective plastic strain rate. The constant *A* is the basic yield stress at low strains while *B* and *n* represent the effect of strain

hardening. The expressions in the second brackets represent the effect of strain rate, where C is the strain rate constant, and $\dot{\varepsilon}_p^*$ is the normalized effective plastic strain rate. The values adopted for the steel are: $A = 7.92\times10^{-1}$ GPa; $B = 5.1\times10^{-1}$ GPa; $n = 0.26$; and $C = 1.4\times10^{-2}$.

Fig. 5. Stress-strain curve for the steel.

- Aluminium (von Mises model): This model uses the original von Mises premise that the yield stress has a constant value: perfectly plastic behaviour. The adopted value for the aluminium is $A = 2.7\times10^{-1}$ GPa of yield stress.

The failure criterion used for the steel was the Johnson-Cook fracture model [21-23]. This failure model is a purely phenomenological model and is based on the plastic strain. The model uses a damage parameter D and when this parameter reaches the value of 1, the ultimate fracture is expected. The definition of the damage parameter is:

$$D = \int \frac{1}{\varepsilon_f} d\varepsilon_{eq}^p \tag{32}$$

where ε_f is the equivalent strain at fracture and $d\varepsilon_{eq}^p$ is the increment of equivalent plastic strain. The expression for the equivalent strain at fracture is given by:

$$\varepsilon_f = \left[D_1 + D_2 e^{-D_3 \frac{\sigma_m}{\sigma_{vm}}} \right] \cdot \left[1 + D_4 \ln\left(\frac{\dot{\varepsilon}_{eq}^p}{\dot{\varepsilon}_0} \right) \right] \tag{33}$$

where D_1, D_2, D_3 and D_4 are material constants (see Table 1), which can be determined from experiments, σ_m is the average of the three normal stresses, σ_{vm} is the von Mises equivalent stress, $\dot{\varepsilon}_{eq}^p$ is the rate of the von Mises plastic equivalent strain and $\dot{\varepsilon}_0$ is a reference strain rate. As can be seen in Eq. (33), the model depends on strain, strain rate and stress triaxiality, where the relationship σ_m/σ_{vm} is a measure of the latter.

Table 1. Parameters used in the current fracture model for the steel.

The failure criterion for the aluminium used in this work is the hydrodynamic tensile failure. In this way a constant hydrodynamic compressive limit is specified for the material. We have chosen a realistic value for this limit of about 1.0 GPa. If the value of the hydrodynamic pressure in a finite element falls below this limit, bulk failure is assumed to have occurred. When this happens, the pressure is set to zero, the internal energy is recomputed and the material is assumed to have healed so that negative pressures may occur in the next time-step but once again limited by the hydrodynamic tensile limit.

The finite element types used in our model are the following [10, 19, 22-23]:

- The bearing ropes and compression sleeves (see Fig. 1 above) were modelled using six faced brick-type (hexahedral) elements with SOLID164.
- Pipe bends (see Fig. 1 above) were modelled using shell element SHELL163.

- CONTA173 and TARGE170 were used in different contact pairs throughout the model, such as between bearing ropes and pipe bends, between compression sleeves and pipe bends and between pipe bends themselves. The contact was modelled as rigid-flexible standard type and the Augmented Lagrange Method (ALM) as the numerical algorithm.

Fig. 6. Finite element types used in the model: (a) SOLID164 element, (b) SHELL163 element, (c) CONTA173 and TARGE170 contact elements and (d) detail of the contact between bearing ropes and pipe bends.

Next, the finite element mesh of the model and details of the contacts are shown in Fig. 7. On the one hand, with respect to the boundary and initial conditions, we have applied a velocity of 5m/s at one of the edges of the brake ring-type energy dissipator, the other edge remaining fixed (zero displacement). On the other hand, three different dynamic friction coefficients, μ_d, have been used in all the contacts of this study: 0.05; 0.10 and 0.12. These three friction coefficients were chosen in order to obtain good agreement between the numerical and experimental results, according to the compression sleeve's tightening pressure.

Fig. 7. Finite element mesh and contact details: (a) Overall mesh, (b) Detail of pipe bend mesh, (c) Detail of compression sleeve mesh, (d) Detail of bearing rope-pipe bend contact, (e) Detail of pipe bend-compression sleeve contact (f) Detail of pipe bend-pipe bend contact.

In order to obtain the solution of the problem, an explicit dynamic analysis procedure is used. Explicit time integration is well suited to contact problems because the small time steps imposed by numerical stability can be used to deal with the discontinuities in the contact problem with different materials. The large time steps made possible by unconditionally stable implicit methods are not effective for discontinuous responses. Furthermore, contact also introduces discontinuities in the Jacobian, which impedes the convergence of Newtonian methods [12-13].

This procedure is based on the implementation of an explicit integration rule together with the use of diagonal or "lumped" element mass matrices. The equations of motion for the body are integrated using the explicit central difference integration rule [1, 12-13, 18]:

$$\dot{\vec{u}}^{\left(i+\frac{1}{2}\right)} = \dot{\vec{u}}^{\left(i-\frac{1}{2}\right)} + \frac{\Delta t^{(i+1)} + \Delta t^{(i)}}{2} \ddot{\vec{u}}^{(i)} \tag{34}$$

$$\vec{u}^{(i+1)} = \vec{u}^{(i)} + \Delta t^{(i+1)} \dot{\vec{u}}^{\left(i+\frac{1}{2}\right)} \tag{35}$$

where $\dot{\vec{u}}$ is velocity, $\ddot{\vec{u}}$ is acceleration and Δt is the time increment. The superscript (i) refers to the increment number and $i-\frac{1}{2}$ and $i+\frac{1}{2}$ refer to mid-increment values. The central difference integration operator is explicit in that the kinematic state can be

advanced using known values of $\dot{\vec{u}}^{(i-\frac{1}{2})}$ and $\ddot{\vec{u}}^{(i)}$ from the previous increment. The explicit integration rule is quite simple but by itself does not provide the computational efficiency associated with the explicit dynamics procedure. The key to the computational efficiency of the explicit procedure is the use of diagonal element mass matrices because the inversion of the mass matrix that is used in the computation for the accelerations at the beginning of the increment is triaxial:

$$\ddot{\vec{u}}^{(i)} = M^{-1} \cdot \left(\vec{F}^{(i)} - \vec{I}^{(i)} \right) \tag{36}$$

where M is the diagonal lumped mass matrix, $\vec{F}$ is the applied load vector, and $\vec{I}$ is the internal force vector. The explicit procedure requires no iterations and no tangent stiffness matrix.

Special treatment of the mean velocities $\dot{\vec{u}}^{(i+\frac{1}{2})}$, $\dot{\vec{u}}^{(i-\frac{1}{2})}$ etc. is required for initial conditions, certain constraints, and presentation of results. For presentation of results, the state velocities are stored as a linear interpolation of the mean velocities:

$$\dot{\vec{u}}^{(i+1)} = \dot{\vec{u}}^{\left(i+\frac{1}{2}\right)} + \frac{\Delta t^{(i+1)}}{2} \ddot{\vec{u}}^{(i+1)} \tag{37}$$

The central difference operator is not self-starting because the value of the mean velocity $\dot{\vec{u}}^{(-\frac{1}{2})}$ needs to be defined. The initial values (at time $t = 0$) of velocity and acceleration are set to zero. We assert the following condition:

$$\dot{\vec{u}}^{\left(+\frac{1}{2}\right)} = \dot{\vec{u}}^{(0)} + \frac{\Delta t^{(1)}}{2} \ddot{\vec{u}}^{(0)} \tag{38}$$

Substituting this expression into the update expression for $\dot{\vec{u}}^{(i+\frac{1}{2})}$ yields the following definition of $\dot{\vec{u}}^{(-\frac{1}{2})}$:

$$\dot{\vec{u}}^{\left(-\frac{1}{2}\right)} = \dot{\vec{u}}^{(0)} + \frac{\Delta t^{(0)}}{2} \ddot{\vec{u}}^{(0)} \tag{39}$$

The explicit procedure integrates through time by using many small time increments. The central difference operator is conditionally stable, and the stability limit for the operator (with no damping) is given in terms of the highest eigenvalue, $\omega_{\max}$, in the system as:

$$\Delta t \le \frac{2}{\omega_{\max}} \tag{40}$$

In this work a small amount of damping is introduced to control high-frequency oscillations. With damping the stable time increment is given by:

$$\Delta t \le \frac{2}{\omega_{\max}} \left(\sqrt{1+\xi^2} - \xi \right) \tag{41}$$

where ξ is the fraction of critical damping in the highest mode. Contrary to our usual engineering intuition, introducing damping into the solution reduces the stable time increment [12].

5. Analysis of results

In the first place, we have calculated the von Mises stress of the entire device for the three friction coefficients. Maximum values of the stresses obtained were: 8.3 GPa for $\mu_d = 0.05$, 1.8 GPa for $\mu_d = 0.10$ and 3.0 GPa for $\mu_d = 0.12$ (see Fig. 8).

Fig. 8. Von Mises stresses for different dynamic friction coefficients for: (a) $\mu_d = 0.05$, (b) $\mu_d = 0.10$ and (c) $\mu_d = 0.12$.

Secondly, we have calculated the energy absorbed in the device both in the three full-scale experimental tests (T1, T2 and T3) and numerical simulations by FEM until its failure.. The results are shown in Table 2. Fig. 9 shows the comparison of experimental tests carried out in our laboratories with the numerical simulation.

Table 2. Comparison of energy absorbed in full-scale experimental tests with energy absorbed obtained by means of numerical simulations by FEM.

Fig. 9. Comparison of experimental tests with numerical simulations.

6. Conclusions

The finite element method has been proven to be a suitable tool in the modelling and analysis of singular structures, such as the analysis of the behaviour of a ring-type brake energy dissipator.

The model analyzed shows important plasticization in the bent (curved) areas of the pipe bends. The main failure mode is due to the hydrodynamic compressive failure mode in the compression sleeves made of aluminium.

A non-linear behaviour is also observed with respect to the structural response of the brake. The dynamic friction coefficient is considered an adjustable parameter in order to obtain good agreement in the values of the absorbed energy between the experimental tests and numerical results.

With respect to the failure models, the hydrodynamic failure model used for the aluminium is more important than the Johnson-Cook failure model for the steel because, in practice, aluminium fails before steel. Besides, this model is very useful and allows calculations to proceed for long periods of time with tensile waves propagating around the system.

An advantage of the explicit algorithms used in this work is that the bodies can be first integrated completely independently, as if they were not in contact. This uncoupled solution correctly indicates which parts of the body are in contact. The contact conditions are imposed after the two bodies have been updated in an uncoupled manner. Thus, no iterations are needed to establish the contact interface

In this work we have used a fine FEM mesh, with a meshing parameter of 0.008m resulting in about 877,000 nodes and 565,000 elements. The minimum time step was 3.16×10^{-9} s and the maximum time step was 10.0×10^{-9} s.

The problem was solved in a workstation computer with an Intel Core2 Duo 6600 @ 2.4 GHz, with 8 GB RAM and 2 TB hard disk. The total CPU time employed for each simulation was 79,500 seconds and the total number of iterations in order to achieve convergence was 95,600.

Acknowledgements

The authors wish to acknowledge the financial support provided by the Department of Construction at University of Oviedo and the GITECO Group. We also thank Swanson Analysis Inc. for the use of the ANSYS University program. Finally, we would like to acknowledge the suggestions made by anonymous reviewers and Dermot Erskine for the English language review.

References

[1] K. Bathe, Finite Element Procedures, Prentice-Hall, New Jersey, 1998.
[2] S.C. Brenner, L.R. Scott, The Mathematical Theory of Finite Element Methods, Springer-Verlag, New York, 2007.
[3] R.D. Cook, D.S. Malkus, M.E. Plesha, R.J. Witt, Concepts and Applications of Finite Element Analysis, Wiley, New York, 2001.
[4] D. Castro-Fresno, J.J. del Coz Diaz, L.A. Lopez, P.J. Garcia Nieto, Evaluation of the resistant capacity of cable nets using the finite element method and experimental validation, Engineering Geology 100(1-2) (2008) 1-10.
[5] J.J. Coz Diaz, P.J. Garcia Nieto, J.A. Vilan, A. Martin, J.R. Prado Tamargo, A. Lozano Martinez-Luengas, Non-linear analysis and warping of tubular pipe conveyors by the finite element method, Mathematical and Computer Modelling 46(1-2) (2007) 95-108.
[6] J.J. Coz Diaz, L.P. Lamarca, P.J. Garcia Nieto, A. L. Martínez-Luengas, J.A. Vilan, Non-linear analysis of a reinforced concrete sheet cover (umbrella) of 40 m diameter by the finite element method, Applied Mathematics and Computation 184(1) (2007) 37-51.
[7] E. Zeidler, Nonlinear Functional Analysis and its Applications IV: Applications to Mathematical Physics, Springer-Verlag, New York, 1988.
[8] J.J. Coz Diaz, P.J. Garcia Nieto, F.P. Alvarez Rabanal, C. Betegon Biempica, Finite element analysis of thin-walled composite two-span wood-based loadbearing stressed skin roof panels and experimental validation, Thin-Walled Structures 46(3) (2008) 276-289.
[9] I.R. Ionescu, J.C. Paumier, On the contact problem with slip displacement friction in elastostatics, International Journal of Engineering Science 34 (1996) 471-491.
[10] T.A. Laursen, Computational Contact and Impact Mechanics, Springer-Verlag, Berlin, 2003.
[11] G. Duvaut, J.L. Lions, Inequalities in mechanics and Physics, Springer-Verlag, Berlin, 1976.
[12] O.C. Zienkiewicz, R.L. Taylor, The Finite Element Method for Solid and Structural Mechanics, Butterworth-Heinemann, New York, 2005.
[13] J.N. Reddy, An Introduction to Nonlinear Finite Element Analysis, Oxford University Press, New York, 2004.
[14] M. Fortin, R. Glowinski, Augmented Lagrangian Methods: Applications to the Numerical Solution of Boundary-Value Problems, Elsevier Science Ltd, Amsterdam, 1983.
[15] R. Glowinski, Numerical Methods for Nonlinear Variational Problems, Springer-Verlag, New York, 2008.
[16] I. Hlavacek, J. Haslinger, J. Necas, J. Lovisek, Solution of Variational Inequalities in Mechanics, Springer-Verlag, Berlin, 1989.

[17] D. Motreanu, M. Sofonea, Quasivariational inequalities and applications in frictional contact problems with normal compliance, Advances in Mathematical Sciences and Applications 10(1) (2000) 103-118.
[18] J.R. Hughes, The Finite Element Method: Linear Static and Dynamic Finite Element Analysis, Dover Publications, New York, 2000.
[19] E. Madenci, I. Guven, The finite element method and applications in Engineering using ANSYS, Springer, Berlin, 2005.
[20] R. Temam, Problèmes Mathématiques in plasticité, Méthodes mathématiques de l'informatique, Gauthiers-Villars, Paris, 1983.
[21] J. Jai-ick Yoh, M.A. McClelland, J.L. Mainenschein, C.M. Tarver, Test-based thermal explosion model for HMX, Proceedings of the Combustion Institute 31 (2007) 2353-2359.
[22] T. Stolarski, Engineering Analysis with ANSYS Software, Butterworth-Heinemann, New York, 2007.
[23] S. Moaveni, Finite Element Analysis: Theory and Application with ANSYS, Prentice Hall, New York, 2007.

Table 1. Parameters used in the current fracture model for the steel.

	Johnson-Cook failure coefficients
D1	0.05+/- 20% standard deviation
D2	3.440
D3	-2.120
D4	0.002

Table 2. Comparison of energy absorbed in experimental full-scale tests with energy absorbed obtained by means of numerical simulations.

Test number (tightening pressure)	Dynamic friction coefficient	Energy in full-scale tests (kJ)	Energy from simulations (kJ)
T1 (12 MPa)	0.05	40	38
T2 (14 MPa)	0.10	32	27
T3 (16 MPa)	0.12	42	44

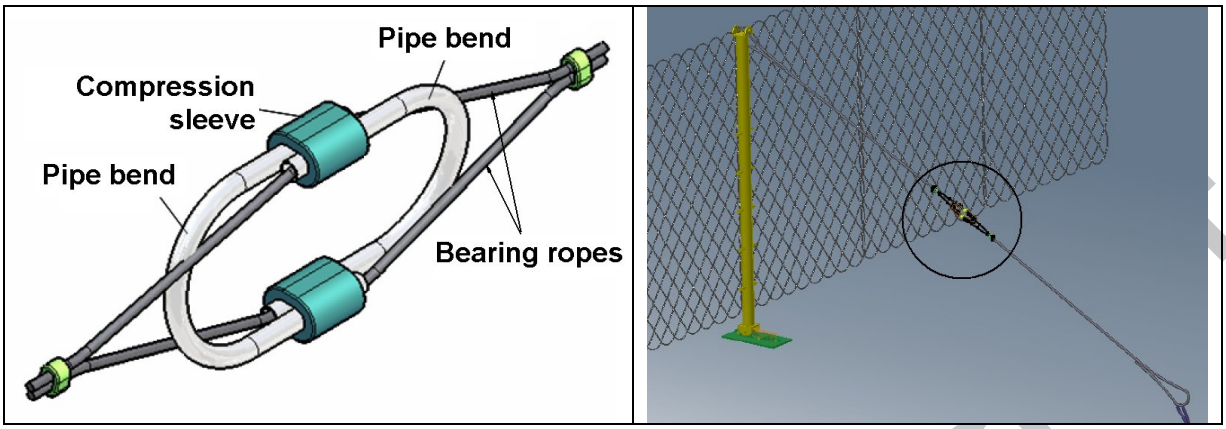

Fig. 1. Geometrical model of the new ring-type brake dissipator (left) and falling rock protection kit (right).

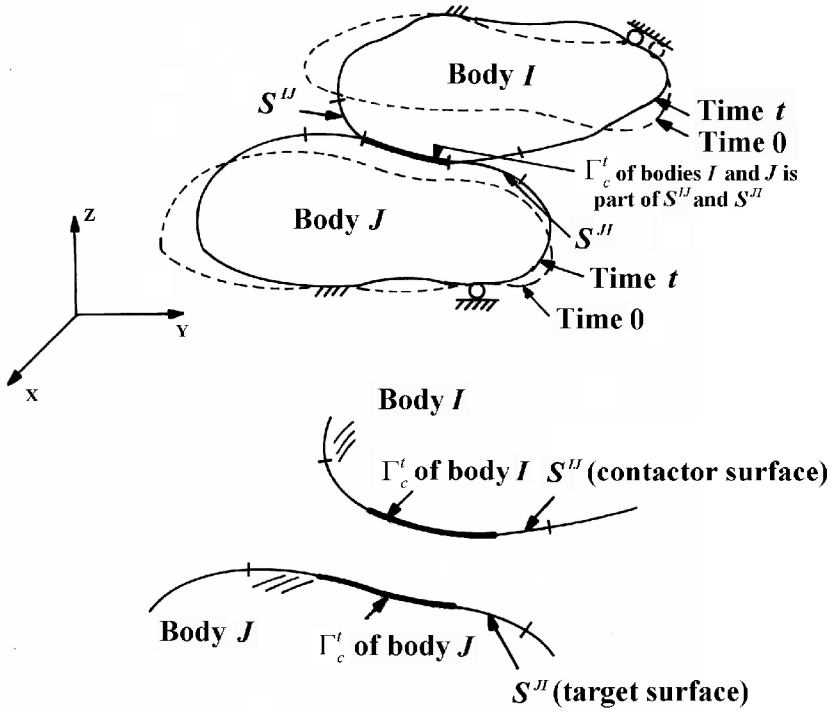

Fig. 2. Bodies in contact at time *t*.

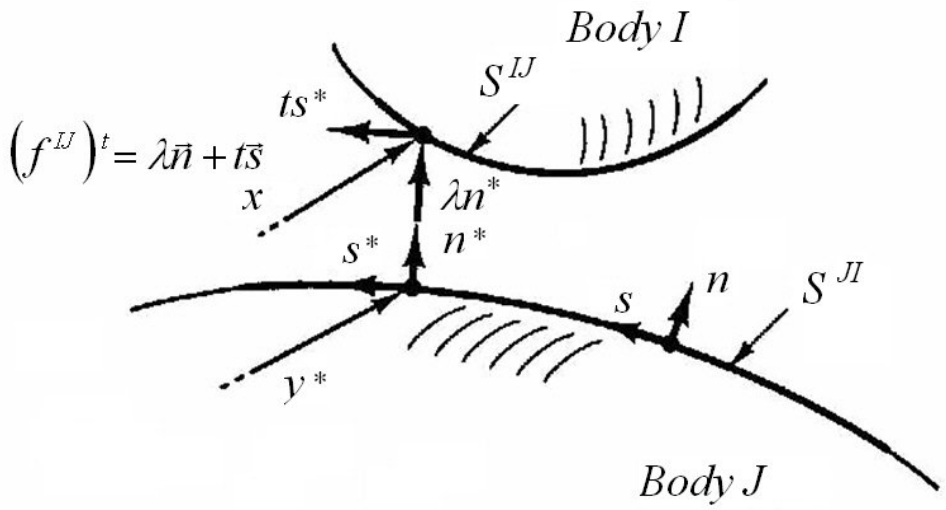

Fig. 3. Definitions used in contact analysis.

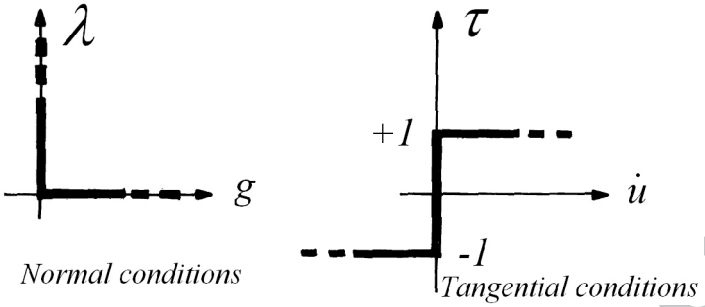

Fig. 4. Interface conditions in contact analysis.

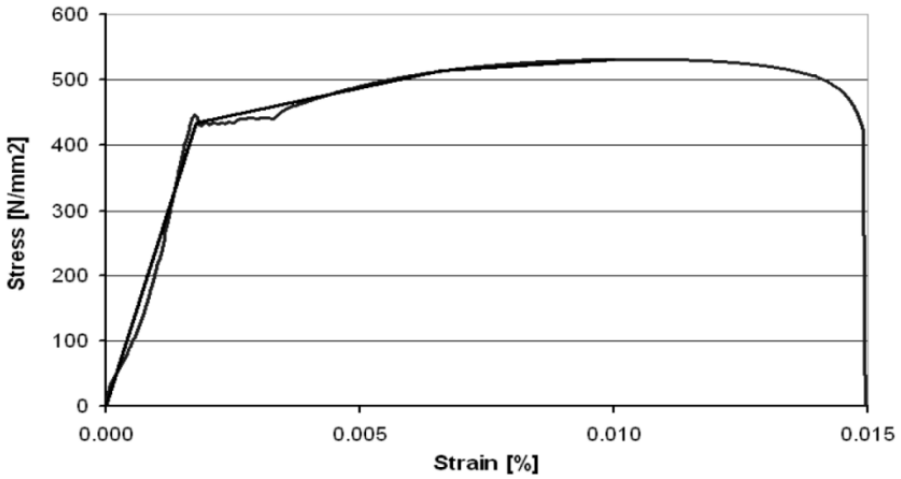

Fig. 5. Stress-strain curve for the steel.

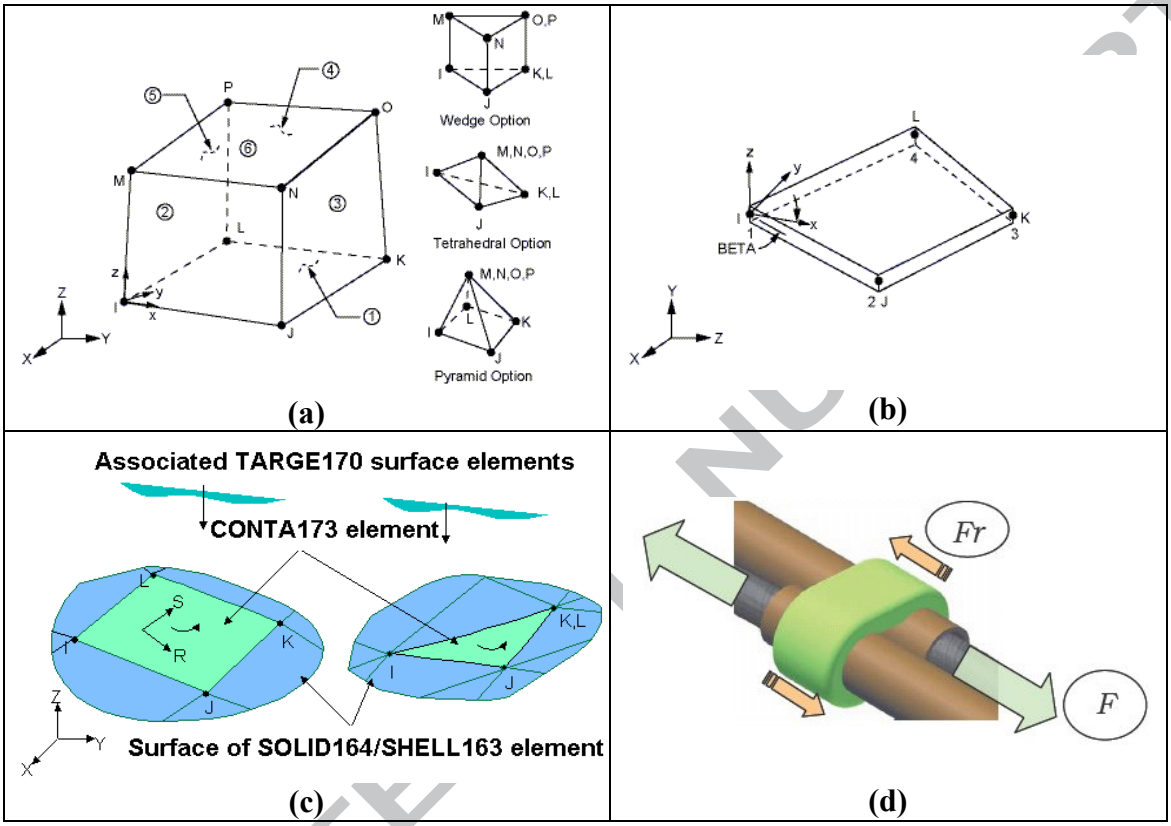

Fig. 6. Finite element types used in the model: (a) SOLID164 element, (b) SHELL163 element, (c) CONTA173 and TARGE170 contact elements and (d) detail of the contact between bearing ropes and pipe bends.

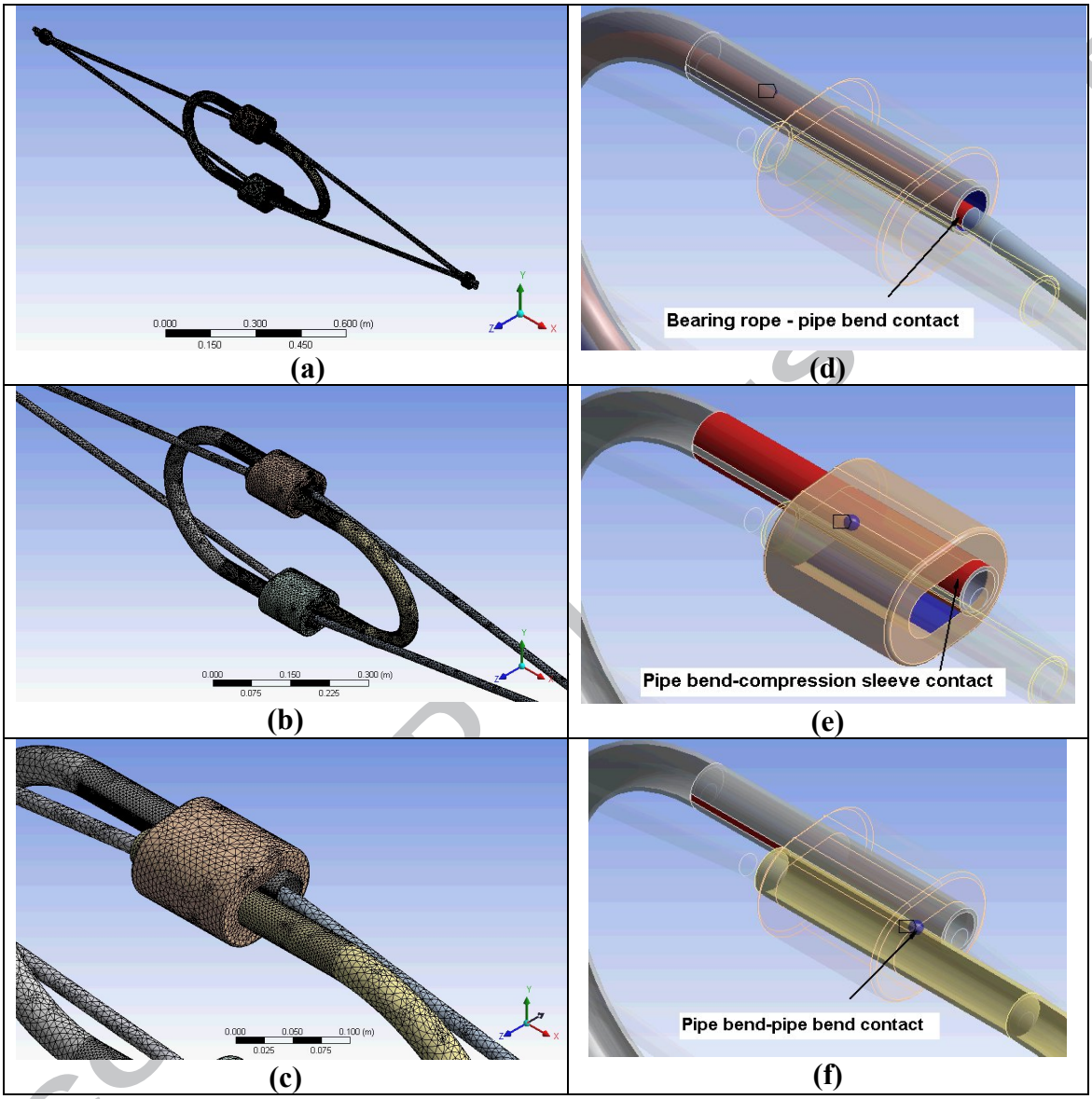

Fig. 7. Finite element mesh and contact details: (a) Overall mesh, (b) Pipe bend mesh's detail, (c) Compression sleeve mesh's detail, (d) Bearing rope-pipe bend contact's detail, (e) Pipe bend-compression sleeve contact's detail and (f) Pipe bend-pipe bend contact's detail.

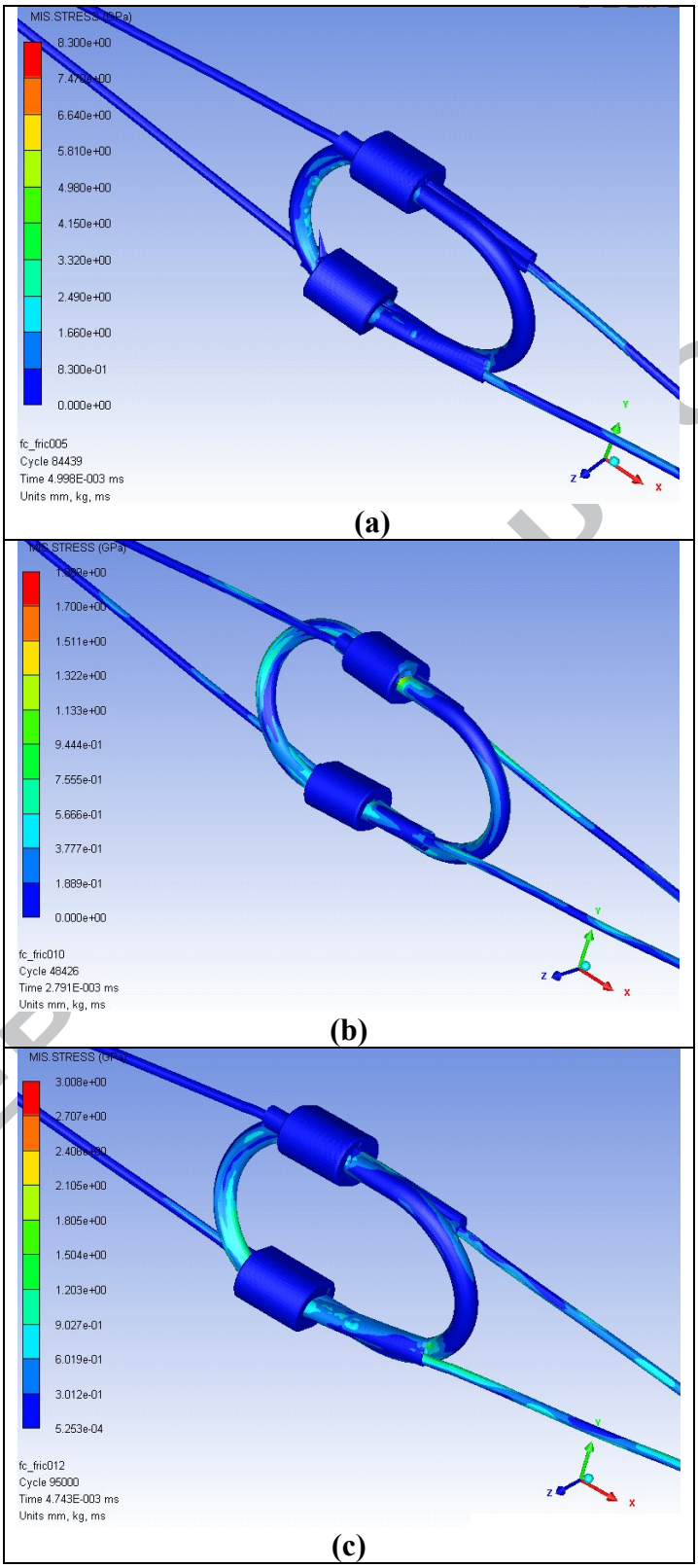

Fig. 8. Von Mises stresses for different dynamic friction coefficients for : (a) $\mu_d = 0.05$, (b) $\mu_d = 0.10$ and (c) $\mu_d = 0.12$.

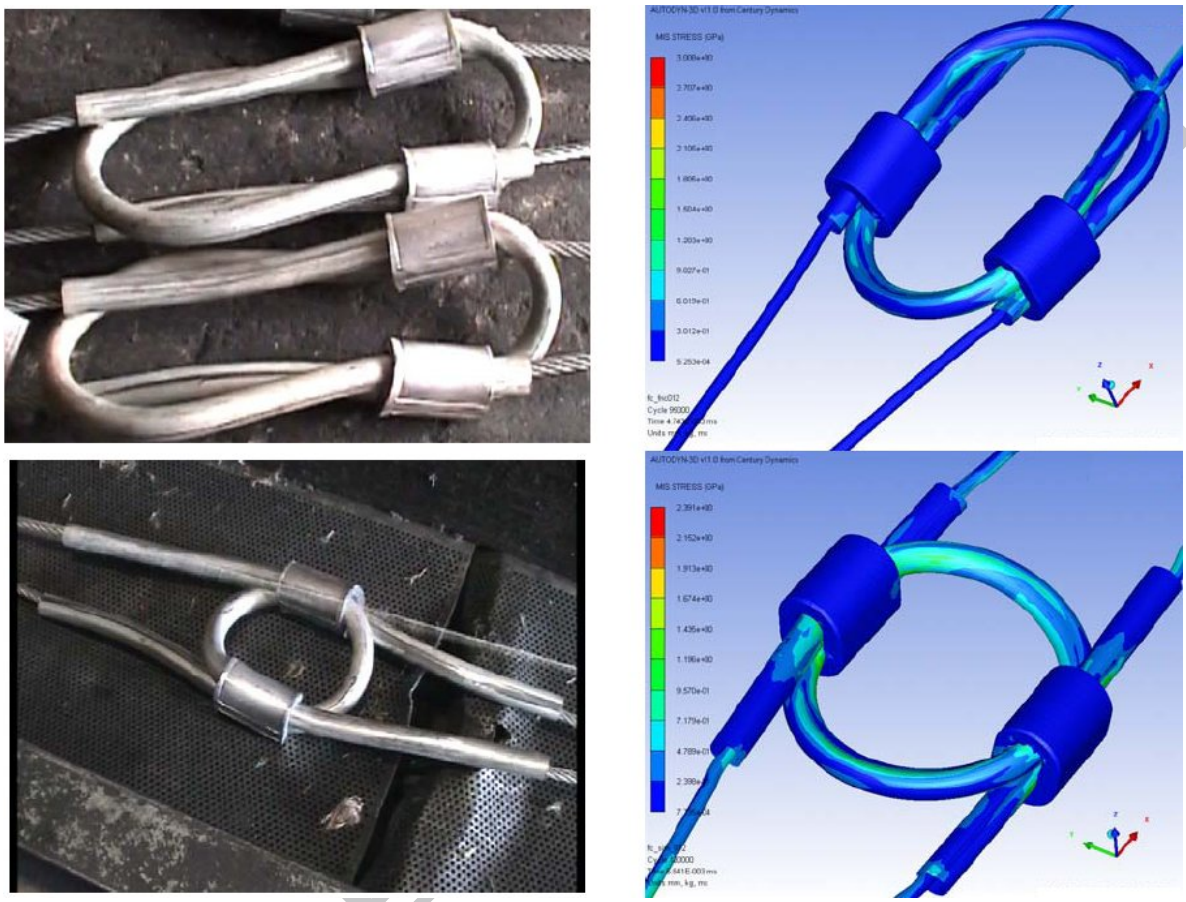

Fig. 9. Comparison of experimental tests with numerical simulations.